aŜǑKƛŜΣ ₩ΦΣ {ǑKǳΝΝΣ .ΦΣ ¸ǳl·ƴΣ ·ΦΣ {ǑKƴŜƛŘŜΝΣ CΦ aΦΣ {ƛLJLJfΣ
/ΦΣ aƛƴl·ŜØΣ ±ΦΣ Dl·ŘƻŜǾΣ aΦΣ hƛϒl·Kϒl·ŘƻØΣ LΦΣ
!ōŘèōl·ǑKl·ŜØΣ ¦ΦΣ aƻfŘƻōŜ˥ƻØΣ .ΦΣ hΝǳƴōl·ŜØΣ {Φ
όнлмфύϒ hōăŜΝØl·ǘƛƻƴă ƻŦ ∃ǳƛŘŜŘ ǿl·ØŜă ŦΝƻϒ ǘKŜ tl·ϒƛΝ
ăŜƛăϒƛǑ ĩƻƴŜ LJΝƻØƛŘŜ l·ŘŘƛǘƛƻƴl·f ŜØƛŘŜƴǑŜ ŦƻΝ ǘKŜ
ŜÈƛăǘŜƴǑŜ ƻŦ ădzōŘdzǑǘŜŘ Ǒƻƴǘƛƴŝƴǘl·f fƻǿŜΝ ǑΝdzăǘΦ π
¢ŜǑǘƻƴƻLJKèăƛǑăΣ тснΣ мπмсΦ

ƘǘǘLJăϒκκŘƻƛΦƻΝ∃кмлΦмлмсκ̯ΦǘŜǑǘƻΦнлмфΦлпΦллт

Observations of guided waves from the Pamir seismic zone provide additional evidence for the existence of subducted continental lower crust

Mechie, J. [a], Schurr, B. [a], Yuan, X. [a], Schneider, F. [a], Sippl, C. [a], Minaev, V. [b], Gadoev, M. [b], Oimahmadov, I. [b], Abdybachaev, U. [c], Moldobekov, B. [c], Orunbaev, S. [c]

[a] Deutsches GeoForschungsZentrum - GFZ, Sections "Geophysical Deep Sounding", "Seismology" and "Lithosphere Dynamics", Telegrafenberg, 14473 Potsdam, Germany
[b] Institute of Geology, Earthquake Engineering and Seismology, Academy of Sciences of the Republic of Tajikistan, Dushanbe 734063, Republic of Tajikistan
[c] Central Asian Institute for Applied Geosciences, 720027 Bishkek, Kyrgyz Republic

Abbreviated title: Guided waves from the Pamir seismic zone

Corresponding author: J. Mechie, Deutsches GeoForschungsZentrum - GFZ, Section "Geophysical Deep Sounding", Telegrafenberg, 14473 Potsdam, Germany. Tel: +49 331 288 1237, Fax: +49 331 288 1266, e-mail: jimmy@gfz-potsdam.de

Keywords: Guided waves, Wave propagation, Continental crust, Central Asia

Highlights

Guided waves from earthquakes within the Pamir seismic zone have been recognized
The guided waves occur as a secondary phase behind the first arrivals
The guided waves are generated by a low velocity layer about 10 km thick
The low velocity layer is caused by subducting lower continental crust
The velocities in the low velocity layer are partly due to the presence of melts

ABSTRACT

As part of the TIPAGE (TIen shan – PAmir GEodynamic program) project, passive seismological observations were made along an approximately N-S profile crossing the Pamir seismic zone for about one year. From these observations guided waves were recognized. These guided waves occur as a single, continuous, secondary, compressional (P) wave phase behind the first P-wave arrivals. An equivalent phase in the shear (S) wavefield is hardly recognizable. Modelling of the phase shows that an approximately 10 km thick low velocity zone (LVZ) between the Moho and about 160 km depth reproduces the guided waves as a single, continuous phase much better than a 15-20 km thick LVZ. Modelling of the arrival times of the guided waves reveals that a model with a P-wave velocity of 6.3 km/s above about 100 km depth, and a velocity of 7.6 km/s between this depth and the deep cluster of earthquakes at about 150 km depth provides the best fit to the observed travel-time data. One plausible way to explain the low velocity of 6.3 km/s is to invoke the presence of melts in the LVZ. Then, taking a velocity of 6.9 km/s for the lower crust being subducted, about 10-13% melt is required to obtain a velocity of about 6.3 km/s in the LVZ between the Moho and about 100 km depth. This would be in keeping with the estimated burial depths from xenoliths of Gondwana terrane affinity brought to the surface in the southeastern Pamir around 11 million yr. ago. The present-day LVZ is interpreted to comprise continental lower crust. Although guided waves are known to exist associated with subducted oceanic crust or fault zones, this is the first time to the knowledge of the authors that guided waves have been observed resulting from a LVZ associated with subducted continental lower crust.

1. Introduction

Guided waves are generally associated with subduction zones and fault zones. Their generation is due to total internal reflection within a low velocity zone associated with, for example, a fault zone or a subduction zone (e.g. Catchings et al., 2016; Garth & Rietbrock, 2017). In some cases they form part of a distorted, dispersive first arrival phase (Abers, 2000; Martin et al., 2003; Garth & Rietbrock, 2014a, b). In other cases they occur as a separate secondary phase clearly separated from the first compressional (P) wave arrival (e.g. Martin et al., 2005; Martin & Rietbrock, 2006; Ellsworth & Malin, 2011; Garth & Rietbrock, 2017; Coulson et al., 2018). In yet other cases and especially when related to fault zones, they have been recognized arriving later than the shear (S) wave phases (Li & Malin, 2008; Catchings et al., 2016). They have been observed at several subduction zones around the Pacific, including Alaska, the Aleutian Islands, the Kurile Islands, Japan, Mariana (Fukao et al., 1983; Hori, 1990; Abers, 2000; Garth & Rietbrock, 2014a, b; Coulson et al., 2018) and Chile (Martin et al., 2003; Martin et al., 2005; Martin & Rietbrock, 2006; Garth & Rietbrock, 2017). They have also been observed at some of Earth's major fault systems e.g. San Andreas fault system (Cormier & Spudich, 1984; Ben-Zion & Malin, 1991; Li & Malin, 2008; Wu et al., 2010; Ellsworth & Malin, 2011), North Anatolian fault (Ben-Zion et al., 2003), Dead Sea Transform (Haberland et al., 2003). Guided waves have also been observed from the Vrancea intermediate depth seismic zone in Romania (Bokelmann & Rodler, 2014), where dispersive first P-wave arrivals have been recognized. The interpretation in this case is that the guided waves have been generated in a low velocity zone associated with the subduction of oceanic crust, now residing at uppermost mantle depths.

In this study, observations of guided waves from the Pamir seismic zone are presented. These guided waves have been observed along the main profile of a passive seismological experiment in the Pamir within the framework of the TIPAGE (TIen shan – PAmir GEodynamic program) project (Mechie et al., 2012; Sippl et al., 2013a, b; Schneider et al., 2013; Schurr et al., 2014a; Kufner et al., 2016; Li et al., 2018). In addition to the observations, an analysis of the travel times and the amplitudes of the first arrivals and guided waves by 2-D ray-tracing (Podvin & Lecomte, 1991) and full waveform, finite-differences seismograms (Kelly et al., 1976) is presented and the results compared with those from other studies of the data from the TIPAGE project.

2. Geological / Tectonic Setting & Previous Work

The Pamir – Hindu Kush seismic zone and the Vrancea seismic zone in Romania are the only two intra-continental regions on Earth with significant seismicity at depths greater than 100 km. As mentioned above, guided waves have also been observed from the Vrancea seismic zone, where Bokelmann & Rodler (2014) interpreted them to have been generated in a low velocity zone associated with the subduction of oceanic crust. However, in the case of the Pamir, subduction of oceanic material should have stopped with the final closure of the Tethys ocean no later than 40 million yr ago (Yin & Harrison, 2000) and thus it is thought that the low velocity zone already detected by a receiver function analysis (Schneider et al., 2013) comprises lower continental crust.

The Pamir forms the northwestern portion of the Pamir-Tibet plateau (Fig. 1), the largest plateau on Earth. The plateau has been formed by the India–Asia continent–continent collision which is also responsible for the Himalayas, the highest mountain range on Earth and deformation in large regions of Central and Eastern Asia (e.g. Tien Shan). Tibet and the Pamir both stand 4-5 km high (Fielding, 1996). In Tibet this topography is supported by a 70–80 km thick crust (Kind et al., 2002; Mechie et al., 2011; Mechie & Kind, 2013) and in the Pamir it is supported by a 65-75 km thick crust (Mechie et al., 2012, Schneider et al., 2013).

Both Tibet and the Pamir have absorbed around 1800–2100 km of Cenozoic N-S shortening (Le Pichon et al., 1992; Johnson, 2002). However, the N-S extent of the Pamir is about 500 km, compared with up to 1300 km for Tibet. Consequently, compared to Tibet, the Pamir has either undergone more lateral extrusion of crust, more erosional unroofing or greater loss of continental crust into the mantle.

The Pamir – Hindu Kush seismic zone would seem to be the obvious place to look for continental crust being lost into the mantle in this region. In the past, some workers understood the Pamir seismic zone to mark about 300 km southward subduction of Asian crust and mantle lithosphere (Hamburger et al., 1992; Burtman & Molnar, 1993), although other workers (Pegler & Das, 1998; Pavlis & Das, 2000) claimed that it represented overturned northward subducting Indian lithosphere. In contrast, the Hindu Kush intermediate-depth seismicity was interpreted to mark around 700 km of subducted Indian lithosphere dipping at about 80° to the north (Negredo et al., 2007). East of the Pamir, Indian lithosphere is 'subducting' beneath Tibet almost horizontally (Kumar et al., 2006; Jiménez-Munt et al., 2008) and may underlie most of western Tibet (Li et al., 2008; Zhao et al., 2010). More recently, the TIPAGE project, through a series of seismological experiments (Mechie et al., 2012; Sippl et al., 2013a, b; Schneider et al., 2013; Kufner et al., 2016; Li et al., 2018), has been able to show that the Pamir seismic zone is due to the southward subduction of Asian continental lithosphere, including lower crustal material, and that the Hindu Kush seismic zone is due to the northward subduction of Indian continental lithosphere. More specifically, the southward subduction of Asian lower crust, which is thought to host the Pamir seismic zone, was initiated about 10 million yr ago when Indian cratonic lithosphere impinged on Asian cratonic lithosphere and, due to the already thickened Pamir crust pushing Asian cratonic lithosphere down, caused it to delaminate and roll back (Kufner et al., 2016). Receiver function analysis has shown that a 10-15 km thick low velocity zone marks the top of the downgoing Asian lithosphere and provided evidence that this low velocity zone hosts the intermediate-depth seismicity and is due to lower continental crust being taken down together with the lithospheric mantle (Schneider et al., 2013). In the receiver function image, the top of the low velocity zone is marked by a negative converter which, by definition, indicates a decrease in velocity downwards (Schneider et al., 2013). Above the low velocity zone, Sippl et al. (2013b) showed that a region with a P-velocity of around 7.1 km/s exists down to a depth of about 100 km. This region was interpreted to be either re-equilibrated felsic, upper crust or meta-stable intermediate, middle crust. Most recently, the Pamir – Hindu Kush seismic zone has been proposed to be a single, contorted slab of Asian origin (Perry et al., 2019). However, this hypothesis is at odds with the uppermost mantle part of the seismicity dipping down to the north beneath the Hindu Kush (Pegler & Das, 1998; Kufner et al., 2016).

The rocks that have been subducted southward may be exemplified by the xenoliths which have been brought up by volcanic rocks about 11 million yr ago in the southeastern Pamir (Hacker et al., 2005 and Fig. 1). These xenoliths comprise mainly eclogites and granulites and a glimmerite. The protoliths for the eclogites were igneous rocks with mafic to felsic compositions whereas the protoliths for the granulites were pelitic sediments (Hacker et al., 2005). The xenoliths are thought to originate from the southern Pamir (Rutte et al., 2017; Schaffer et al., 2017) which is thought to be the lateral equivalent of one of the Gondwana terranes, namely the Lhasa terrane, in Tibet (Schwab et al., 2004). They are thought to have been taken down to 90-100 km depth due to transient crustal drips and subduction erosion, before being brought up to the surface (Hacker et al., 2005; Rutte et al., 2017). The crustal rocks subducting at the present day as part of the Pamir seismic zone are thought to belong to Asian cratonic lithosphere (Kufner et al., 2016) and thus they have no affinity with the Gondwana terrane, from which the xenoliths were derived. However, as long as the rock types are similar, then the processes that operated on the xenoliths in the past may very well be occurring in the present-day Pamir seismic zone.

3. Characteristics of Guided Waves, Background Model, Earthquake Selection & Processing

The guided waves observed in this study mainly occur as secondary arrivals in the P-wavefield (Figs. 2-4). They cannot be observed nearly so well in the S-wavefield, although in some cases it is possible that they are present. A dispersion analysis was carried out for the data recorded by the vertical component at two stations (P08 & P09, Figs. 2-3) for two events (302 & 304, Table 1). A frequency-time analysis was carried out following Dziewonski et al. (1969), using 60 different filters centred between 0.67 and 10 Hz. The frequency-time plots (Fig. 5) show that the guided waves are more prominent at lower frequencies whereas for event 302 the first arrivals are more prominent at higher frequencies. For the guided waves there is no smooth, consistent dependence of arrival time on frequency for any of the four analysed traces, although the trace at station P09 from event 302 may show some dependence. Although guided waves are dispersive in nature and this dispersion is often observed (e.g. Abers, 2000; Martin et al., 2003; Ellsworth & Malin, 2011; Garth & Rietbrock, 2014a, b; Bokelmann & Rodler, 2014, Coulson et al., 2018), there are cases where dispersion is not observed (e.g. Haberland et al., 2003).

All the velocity models (Figs. 6 and S1-S2) that are utilized in this study for calculating the travel times and amplitudes of the seismic waves incorporate, as the background model, a 2-D cross-section close to the TIPAGE main profile through the 3-D model derived from local earthquake tomography (Fig. 7 and cross-section D-D’ in Fig. 2 of Sippl et al., 2013b). In addition, the Moho and the boundaries of the low velocity zone hosting the Pamir seismic zone were based in the initial test models on converters identified by a receiver function analysis (red lines in Fig. 7 and Fig. 6 in Schneider et al, 2013). The boundaries of the low velocity zone were slightly modified during the modelling process so that most of the earthquakes occurred in the top half of the seismic zone.

Earthquakes which show guided waves and which are located close to the TIPAGE main profile were utilized in this study. 13 earthquakes fulfilled these requirements (Table 1). The waveforms of the different events recorded at the same station are often quite similar but there are differences in detail. For example, although station P08 always shows a pickable guided wave phase (Figs. 2-4), for events 318 and 325 the amplitude of the guided wave phase is smaller than that of the first arrival whereas for the other events the amplitude of the guided wave phase is larger than that of the first arrival. The earthquake hypocentres were derived by relocating them, from the original catalogue provided by Sippl et al. (2013a), in the 3-D model derived from local earthquake tomography (Sippl et al., 2013b), as a 2-D cross-section through this model was utilized as the background model in the present study. The earthquakes were then projected onto the TIPAGE main profile (Fig. 1). A comparison between the theoretical 1st arrival times derived from the 3-D model of Sippl et al. (2013b), the 2-D background model utilized in this study (Fig. 7) and one of the 2-D models incorporating a low velocity zone (model 2 in Fig. 6) was made (Fig. S3). This comparison shows that in the portion of the profile where the guided waves are observed, the travel-time differences between the three models are generally less than 0.4 s. Power spectra were calculated for two of the events (302 & 304, Table 1) which showed well-developed guided waves. These spectra showed a peak between 1 and 2 Hz. Thus the record sections were band-pass filtered between 0.1 and 2 Hz. Then the arrival times for both the first arrivals and the guided waves were picked.

4. Modelling of Travel Times of Guided Waves

Synthetic seismograms were calculated using a finite-difference approximation of the wave equation for 2-D heterogeneous elastic media by Kelly et al. (1976) with transparent boundary conditions (Reynolds, 1978) and implemented by Sandmeier (1990). Firstly, synthetic seismograms were calculated for the background model to examine if it would produce guided waves. For this model and the models described in this and the following paragraph, an explosive point source with a dominant frequency of 1.25 Hz in combination with a Fuchs-Müller signal (Fuchs & Müller, 1971) was used. The model is stable up to a frequency of 5 Hz, as are all the models in this study. The background model did not produce any guided wave energy. Then the converters bounding the low velocity zone identified by Schneider et al. (2013) were added to the background model. This resulted in a 15-20 km wide zone between the bounding converters (blue lines in Fig. 7). In addition, Schneider et al. (2013) recognized that the velocity in the zone between the converters should be less than that of the surrounding mantle material as the polarity of the upper converter meant that it represented a velocity decrease with depth while the polarity of the lower converter meant that it represented a velocity increase with depth. Thus, a P-velocity of 6.9 km/s was assigned to the low velocity zone (LVZ) between the converters. This was based on the average for the basal 10-15 km of the crust from the interpretation of refracted and wide-angle reflected phases along the profile (Mechie et al., 2012). Using this model synthetic seismograms were calculated for a number of synthetic sources including sources inside the LVZ and sources outside the LVZ, both above and below it. It was found that sources below the LVZ produced little or no guided wave energy (Fig. S1, middle right). Sources within or above the LVZ produced energy behind the first arrivals similar to that in the observed data. For sources far enough above the LVZ, the strong secondary arrivals are at least in part due to strong reflections from the base of the LVZ (see e.g. the distance range from 110-160 km in Fig. S1, upper right). For sources within the LVZ, the secondary energy was often split into two distinct phases (Fig. S1, middle left) while in the observed data the secondary phase looks like one long continuous phase. This was taken to indicate that the LVZ was too wide. Thus the width of the LVZ was reduced to about 10 km in the next model (black lines in Fig. 7). Actually, forward waveform modelling of receiver functions for six stations in the vicinity of the southern part of the profile revealed a thickness of 10-15 km for the LVZ (Schneider et al., 2013).

Tests with synthetic sources for an approximately 10 km wide LVZ showed that the synthetic secondary energy mimicked the observed secondary energy best in terms of looking like one long continuous phase rather than two split phases, when the synthetic source was located in the upper half of the LVZ (Fig. S1, lower right). The top boundary of the LVZ was thus modelled so that the 13 real earthquakes would lie, if possible, in the upper half of the LVZ. Without introducing a concave element to the top boundary of the LVZ, it was possible to have all except the deepest earthquake of the middle cluster of events in the upper half of the LVZ (Fig. 7). Further, the two boundaries of the approximately 10 km wide LVZ lie mainly within the bounds defined by the converters identified by the receiver function analysis of Schneider et al. (2013). With this configuration of boundaries for the approximately 10 km wide LVZ in relation to the 13 real earthquakes, the one remaining parameter to be determined is the velocity within the LVZ.

The velocity within the LVZ primarily controls the travel-time difference between the first arrivals and the secondary guided wave energy travelling through the LVZ. Thus models were constructed in which the velocity in the LVZ above about 130 km depth was varied in 0.1

km/s steps from 6.2 to 6.9 km/s for the shallow earthquake and from 6.3 to 6.9 km/s for all other events. This results in velocity gradients along the dip direction of the LVZ for these models and, in fact, for any of the models in this study of up to 0.05 km/s/km. As the power spectra of the observed data showed a peak between 1 and 2 Hz, for these and all subsequent models the dominant frequency of the explosive point source was 1.5 Hz and the resulting bandwidth of the signal is from 0.8 to 3.5 Hz. At depths greater than about 160 km the LVZ was constrained to disappear as the receiver function study of Schneider et al. (2013) showed that the converters marking the top and bottom boundaries of the LVZ disappear at about this depth and the study of Sippl et al. (2013a) showed that the seismicity also disappears at about this depth. For each of the constructed models synthetic seismograms were calculated for the 13 earthquakes (Fig. 8). Then the travel times of the synthetic secondary guided wave arrivals were picked and compared with the travel times of the observed secondary guided wave arrivals. The picking was done on record sections with 15 km station spacing, which is approximately the same as the station spacing in the observed data. Further, only phases that have a significant amplitude compared to that of the first arrival were picked, as only such phases could be picked in the observed data. This sometimes meant that the earliest guided wave arrival was not picked as it was too weak, but a later more prominent arrival (Fig. 8c-d). When comparing the absolute travel times of the observed and theoretical guided waves, the model (model 1 in Fig. 6) with the smallest root mean square residual time (trms), was that in which the LVZ had a velocity of 6.7 km/s above about 130 km depth (Fig. 9). In addition, the travel times of the synthetic first arrivals were calculated using finite-differences ray-tracing based on the eikonal equation (Vidale, 1988; Podvin & Lecomte, 1991; Schneider et al., 1992). Then the differences between the synthetic secondary guided wave arrivals and first arrivals were calculated and compared with the differences between the corresponding observed arrivals. In this case, the model with the smallest root mean square residual time (trms), was that in which the LVZ had a velocity of 6.6 km/s (model 1a) instead of 6.7 km/s (model 1) above about 130 km depth.

During this analysis it was realized that the shallow earthquake (Fig. 4) required the smallest average velocity (6.3 km/s), whereas the intermediate cluster of earthquakes (Fig. 3) required a greater average velocity (6.4 – 6.6 km/s) and the deep cluster of earthquakes (Fig. 2) required the largest average velocity (6.9 km/s or even larger). Thus a model (model 2 in Fig. 6) was made with varying velocity in the LVZ. Above the shallow earthquake a velocity of 6.3 km/s was assigned to the LVZ, whereas between the shallow earthquake and the deep cluster of earthquakes a velocity of 7.6 km/s was assigned. This resulted in a trms which was smaller than those for the cases where the LVZ had a velocity of 6.6 or 6.7 km/s above 130 km depth. However, this model only has one change in velocity between the shallow earthquake and the deep cluster of earthquakes whereas, as mentioned above, the average velocities required to fit the observed travel-time data imply that there may be an additional change in velocity between the intermediate and deep clusters of earthquakes. For this reason a further model (model 3 in Fig. 6) was made with varying velocity in the LVZ. In this case, the velocity above the shallow earthquake was assigned a value of 6.4 km/s, the velocity between the shallow earthquake and the intermediate cluster of earthquakes was assigned a value of 7.2 km/s and the velocity between the intermediate and deep clusters of earthquakes was assigned a value of 7.6 km/s. This resulted in a trms which was smaller than those for models 1 or 1a but larger than that for model 2. Thus, from the point of view of the travel times, model 2 has the smallest trms and is thus considered to be the best model. Snapshots (Fig. 10) and an animation (Video S1) of waves propagating through this model for event 304 are presented. These snapshots and animation are representative of wave propagation in all the models with an approximately 10 km wide LVZ, for events in the upper half of the LVZ. A digital version of this model (Data Set S1) is also presented.

5. Modelling of Amplitudes of Guided Waves

The amplitudes of the first arrivals and the secondary guided wave phase were picked in the observed data, filtered from 0.1 to 2 Hz, of the 13 earthquakes (see e.g. Figs. 2-4). For the model (model 1) in which the LVZ had a velocity of 6.7 km/s above about 130 km depth and for the two models (models 2 & 3) with varying velocities in the LVZ, the amplitudes of the first arrivals and the secondary guided wave phase were picked in the synthetic data of the 13 earthquakes (see e.g. Fig. 8). The bandwidth of these synthetic data is from 0.8 to 3.5 Hz and is thus similar to that of the observed data. Then the amplitude ratios of the secondary guided wave phase to the first arrival phase were calculated for both the observed and synthetic data and compared (Fig. 11). The differences in amplitude ratios between the observed and synthetic data for all 13 earthquakes for each of the three models were calculated. Although model 3 (Fig. 6) had the smallest root mean square (rms) amplitude ratio difference, the difference between the three models is very small with all three models having a rms amplitude ratio difference between 1.6 and 1.62. Thus amplitudes did not help in the present study to decide which model is to be preferred. On the other hand, a more detailed study of the amplitudes should probably also better approximate the radiation pattern of the real sources rather than employing a simple explosive point source as in the present study.

6. Discussion

The fact that the earthquakes at 100-160 km depth in the Pamir seismic zone generate guided waves is important, as it has implications for the physical properties of the seismic zone. The presence of second arrivals behind the first arrivals suggests that a zone of low or high velocity exists with fairly sharp transitions with respect to the wavelength, to the materials above and below the zone. Although guided waves are really associated with low velocity zones, when a model was made in which the low velocities were replaced by high velocities of, for example, 8.8 km/s, second arrivals similar to the guided waves actually appeared behind the first arrivals, even though these second arrivals are not actually guided waves (Fig. S2). Interestingly, in the synthetic seismograms for event 304 for this model, the second arrival phase does not separate from the first arrivals until 150-200 km distance and the time difference between the two phases at 250 km distance is only about 2 s. This is in contrast to the observed data where the guided wave phase appears as a separate phase at 80-100 km distance and the time difference between the first arrivals and the guided waves at about 250 km distance is 5-6 s (see Fig. 3a). In the case of the Pamir, there are other lines of evidence pointing to a low velocity zone (LVZ) rather than a high velocity zone. The first line of evidence is from the receiver function analysis of Schneider et al. (2013), who imaged two converters bounding the Pamir seismic zone. Additionally, as mentioned in section 4 above, the two converters defined a LVZ in the region between them. The second line of evidence is from the local earthquake tomography study of Sippl et al. (2013b), whose results are also compatible with a LVZ in the vicinity of the Pamir seismic zone. From a geological point of view it is also reasonable to expect a LVZ associated with the Pamir seismic zone, if the lowermost crustal layer has stayed attached to the underlying downgoing mantle layer. This is because the lowermost crustal layer will have a lower velocity than the underlying and overlying mantle material.

When comparing the observations of guided waves made in this study with those made at oceanic subduction zones the different geometries of the experimental setups come to mind. At oceanic subduction zones where the situation is rather similar, with the oceanic crust acting as a low velocity waveguide on top of the oceanic mantle lithospheric slab, guided waves are only observed on land if there is a feature that allows them to leave the waveguide. In the case of Chile this is a kink in the slab in one case (Martin et al., 2003; Martin & Rietbrock, 2006; Garth & Rietbrock, 2017) and an equalization in seismic velocities in another case (Martin et al., 2005). The equalization in seismic velocities occurs when the oceanic crust comes in contact with continental crust, usually lower continental crust, which has similar seismic velocities. In the case of Japan it is also a kink in the slab in one case (Garth & Rietbrock, 2014b) and an equalization in seismic velocities in other cases (Fukao et al., 1983; Hori, 1990). If this feature is not present, the guided waves follow the waveguide to the trench, where usually no stations are located. In this study, there is a much better station coverage around the waveguide since there is no ocean involved and the waveguide terminates into the overlying lower crust.

From an analysis of receiver functions recorded by six of the stations above the Pamir seismic zone, Schneider et al. (2013) determined that the LVZ is 10-15 km thick. From further analysis at one of the stations (P18, Fig. 1), Schneider et al. (2013) concluded that the LVZ has a S-wave velocity of about 4.16 km/s. Assuming a Poisson’s ratio greater than 0.22, this is equivalent to a P-wave velocity greater than 6.94 km/s. The depth for which this velocity within the LVZ was obtained is about 100 km, due to the position of the station with respect to the Pamir seismic zone and the incidence angles of the incoming waves. In the present study a thickness of 10 km for the LVZ was found to better reproduce the appearance of the guided waves as a single secondary phase than a thickness of 15-20 km. With respect to the P-wave velocities at 100 km depth, the best models (model 1 or model 1a) with a uniform velocity in the LVZ above about 130 km depth had a velocity of 6.6 or 6.7 km/s, whereas model 3 (Fig. 6) had a velocity of 6.8 km/s, and model 2 (Fig. 6) with the smallest root mean square residual time (trms) had a velocity of 7.0 km/s. Thus the model with the smallest trms also has a velocity at 100 km depth in the LVZ which is closest to that derived from the receiver function analysis, assuming a Poisson’s ratio of 0.22 or greater.

From a local earthquake tomography study, Sippl et al. (2013b) found P-wave velocities of around 7.1 km/s between 60 and 100 km depth on top of the high-velocity, south-dipping lithospheric mantle slab. At 100 km depth model 2 (Fig. 6), with the smallest trms, has a velocity in the LVZ which is closest to the value of 7.1 km/s obtained by Sippl et al. (2013b). However, at shallower depths of, for example, about 70 km the models (model 1 or model 1a) with a uniform velocity of 6.6 or 6.7 km/s in the LVZ above about 130 km depth have a velocity closer to the value of 7.1 km/s obtained by Sippl et al. (2013b), as models 2 and 3 have velocities of 6.3 and 6.4 km/s in the LVZ at about 70 km depth. A similar argument can be made if one compares the P-wave velocities in the LVZ derived in this study with the average P-wave velocity of about 6.9 km/s for the basal 10-15 km of the crust from the interpretation of refracted and wide-angle reflected phases along the TIPAGE main profile (Mechie et al., 2012). The models (model 1 or model 1a) with a uniform velocity of 6.6 or 6.7 km/s in the LVZ above about 130 km depth show a difference of just 0.2 or 0.3 km/s with respect to the average P-wave velocity of 6.9 km/s derived for the basal 10-15 km of the crust by Mechie et al. (2012). Models 2 and 3, with laterally varying velocities, have velocities of 6.3 and 6.4 km/s above about 90 km depth in the LVZ. Only at about 100 km depth do models 2 and 3 have velocities in the LVZ closer to the average P-wave velocity of 6.9 km/s derived for the basal 10-15 km of the crust by Mechie et al. (2012), than the models (model 1 or model 1a) with a uniform velocity of 6.6 or 6.7 km/s in the LVZ above about 130 km depth. One caveat in this case is that the velocity in the basal 10-15 km of the crust varies laterally and then the velocity in the LVZ need not agree with the average P-wave velocity of 6.9 km/s derived for the basal 10-15 km of the crust by Mechie et al. (2012) along the TIPAGE main profile. In summary, a model with laterally varying velocities in the LVZ fits the travel times of the guided waves or the travel-time differences between the guided waves and the first arrivals best. However, a model with a uniform velocity of 6.6-6.7 km/s (model 1 or 1a) in the LVZ above about 130 km depth may seem, from a first point of view, to fit better with other geophysical results along the TIPAGE main profile and may appear to be the most reasonable model from a geological point of view.

Inaccuracies in the hypocentres of the events are one possible source of error in determining the travel times of the arrivals and hence the velocity distribution in the LVZ. In order to study the effects of possible errors in the hypocentres of the events, the event 330 was moved 4.4 km to the south and 7 km deeper, so that it is again located just below the upper boundary of the LVZ. Then synthetic seismograms were calculated for the relocated event in model 1. First arrivals were calculated as described above using finite-differences ray-tracing and the second arrivals of the guided wave phases were picked. Then the differences between the synthetic secondary guided wave arrivals and first arrivals were compared with the differences between the corresponding observed arrivals. The comparison shows that the trms is 0.972 s. This value is smaller than the value of 1.399 s for the original hypocentre of the event. It lies between the values of 1.062 s for a velocity of 6.5 km/s in the LVZ and 0.939 s for a velocity of 6.4 km/s in the LVZ for the original hypocentre of the event. Thus moving the event 4.4 km to the south and 7 km deeper results in a trms which is equivalent to that for the original hypocenter for a velocity in the LVZ reduced by 0.2-0.3 km/s. This is a step in the correct direction to reducing the overall misfit between the observed and synthetic data. However, the skew in the first arrival times at the stations within about 50 km of the epicentre is definitely noticeable, due to the small station spacing of about 15 km in the N-S direction along the TIPAGE main profile (Fig. S4). This skew is unreasonable and thus it is concluded that errors in the hypocentres are not a major factor in producing errors in the travel times of the arrivals and especially the travel-time differences between the secondary guided wave arrivals and first arrivals. Thus the problems in determining the velocities in the LVZ should have other sources in addition to the possible, relatively modest ones introduced by the inaccuracies of the hypocentres of the events.

There is perhaps one way to explain the variable velocities found in either models 2 or 3 in the LVZ that is geologically reasonable. As mentioned above, Hacker et al. (2005) studied a suite of xenoliths from the southeastern Pamir (Fig. 1) that were brought to the surface by volcanic rocks about 11 million yr ago. This suite consists of eclogites for which the protoliths were igneous rocks with mafic to felsic compositions and granulites for which the protoliths were pelitic sediments. In the transformation of these rocks to eclogites and granulites, high-pressure dehydration melting took place. The favoured scenario of Hacker et al. (2005) was that the igneous and sedimentary rocks were being subducted when they were metamorphosed to eclogites and granulites and that the melts released during this transformation migrated back up the subduction zone, which would essentially be the LVZ in this study. Assuming that this process is occurring in the slab presently subducting and that the melts are concentrated above about 100 km depth (Fig. 12), then this might explain the low average velocity in the LVZ required by the shallowest event, 330. Taking a P-wave velocity of around 3.45 km/s at about 85 km depth for the melt (Stolper et al., 1981) and a P-wave velocity of 6.9 km/s for the lower crust being subducted, then about 10-13% melt (e.g. Watt et al., 1976) is required to obtain an average velocity of about 6.3 km/s (Fig. 12). This is the average velocity which best fits the data from the shallowest event, 330 (Fig. 9). The presence of melt in the LVZ may also help to explain why there are almost no earthquakes between the Moho and 90 km depth in this part of the Pamir seismic zone (Sippl et al., 2013a). It is also in agreement with high seismic attenuation being observed in this region (Schurr et al., 2014b). That the melts concentrate in the LVZ above 100 km depth may be due to the possible tensional forces which probably exist in this depth range as the lower crust is bent down from the north into the Pamir seismic zone. Such forces are thought to exist and to cause faulting in the oceanic crust as it enters a subduction zone (see e.g. Garth & Rietbrock, 2014a and references therein). There remains the question of why the melts remain confined to the LVZ and do not migrate either into the lower crust above the Moho to the north of the subducting slab or into the meta-stable middle crust of Sippl et al. (2013b) lying immediately above the subducting lower crust (Fig. 12). The simplest explanation is that the melts are lighter than the lower crust once it is part of the subducting slab but are heavier than both the lower crust before it is part of the subducting slab and the meta-stable middle crust above the subducting lower crust.

7. Conclusions

In this study, observations of guided waves from the Pamir seismic zone have been presented. These guided waves occur as secondary P-wave arrivals behind the first P-wave arrivals. Equivalent arrivals in the S-wavefield are much less readily observable. Four traces were analysed for dispersion, but the guided wave phases only showed signs of any dispersion in one of these cases.. A 10 km thick low velocity zone (LVZ) reproduces the guided waves as a continuous, single phase much better than a 15-20 km thick LVZ. Along the TIPAGE main profile, the LVZ exists down to about 160 km depth. Modelling of the velocities in the LVZ shows that for models with a constant velocity in the LVZ above about 130 km depth, the model (model 1 in Fig. 6) with a velocity of 6.7 km/s produced the smallest root mean square residual time (trms) when modelling absolute travel times of the guided waves. In contrast, the model with a velocity of 6.6 km/s produced the smallest trms when modelling the travel-time differences between the guided waves and the first arrivals. However, among the models tested, the smallest trms is realized by a model (model 2 in Fig. 6) with a velocity of 6.3 km/s above about 100 km depth and a velocity of 7.6 km/s between the shallow event and the deep cluster of earthquakes at about 150 km depth. Modelling of the amplitudes did not help to discriminate further between the three best travel-time models (models 1, 2 and 3 in Fig. 6). If a lateral change in composition of the lowermost crust is not responsible for a velocity reduction from 6.9 km/s, as derived for the basal 10-15 km of the crust to the north of the LVZ (Mechie et al., 2012), to 6.3 km/s in the LVZ above 100 km depth, then one plausible way to explain the low value of 6.3 km/s is to invoke the presence of melts in the LVZ. Then, taking a velocity of 6.9 km/s for the lower crust being subducted, about 10-13% melt is required to obtain an average velocity of about 6.3 km/s in the LVZ between the Moho and about 100 km depth. This would be in keeping with the results of Hacker et al. (2005), who studied xenoliths with Gondwana terrane affinity brought to the surface in the southeastern Pamir about 11 million yr. ago. Hacker et al. (2005) proposed that during the formation of these eclogitic and granulitic xenoliths, high-pressure dehydration melting took place and that these melts migrated back up the subduction zone. Although the present-day LVZ is associated with the subduction of material with Asian affinity it is possible that the same processes that operated in the Pamir about 11 million yr. ago are again presently active. Thus the present-day LVZ is interpreted to comprise continental, lower crustal material. Although there are a number of studies of guided waves resulting from LVZs associated with subducted oceanic crust or fault zones, this is the first time to the knowledge of the authors that guided waves have been observed resulting from a LVZ associated with subducted continental lower crust.

Acknowledgments

The TIPAGE project was funded by the Deutsches GeoForschungsZentrum – GFZ, Potsdam and the Deutsche Forschungsgemeinschaft (bundle 443, projects RI1127/8, RA442/34). The instruments used in the field program were provided by the Geophysical Instrument Pool of the Deutsches GeoForschungsZentrum – GFZ, Potsdam. The data from the instruments (FDSN code 7B 2008-2010) are archived at the GEOFON data centre (Yuan et al., 2008). These data are publicly available. Thanks to T. Ryberg for doing the dispersion analysis of the guided waves and to B. Hacker for discussion on the melting of the xenoliths. Many of the figures were prepared with the help of the GMT plotting routines (Wessel & Smith, 1991)

References

Abers. G.A., 2000. Hydrated subducted crust at 100-250 km depth. Earth Planet. Sci. Lett.176, 323-330.

Ben-Zion, Y., Malin, P., 1991. San Andreas fault zone head waves near Parkfield, California. Science, 251, 1592-1594.

Ben-Zion, Y., Peng, Z., Okaya, D., Seeber, L., Armbruster, J.G., Ozer, N., Michael, A.J., Baris, S., Aktar, M., 2003. A shallow fault-zone structure illuminated by trapped waves in the Karadere-Duzce branch of the North Anatolian Fault, western Turkey. Geophys. J. Int. 152, 699-717.

Bokelmann, G., Rodler, F.-A., 2014. Nature of the Vrancea seismic zone (eastern Carpathians) – New constraints from dispersion of first-arriving P-waves. Earth Planet. Sci. Lett.390, 59-68. doi:10.1016/j.epsl.2013.12.034.

Burtman, V.S., Molnar, P., 1993. Geological and geophysical evidence for deep subduction of continental crust beneath the Pamir. Special Paper 281, Geological Society of America, Boulder, Colorado.

Catchings, R.D., Goldman, M.R., Li, Y.-G., Chan, J.H., 2016. Continuity of the West Napa – Franklin Fault Zone inferred from guided waves generated by earthquakes following the 24 August 2014 Mw 6.0 South Napa earthquake. Bull. seism. Soc. Am. 106, 2721-2746. doi:10.1785/0120160154.

Cormier, V.F., Spudich, P., 1984. Amplification of ground motion and waveform complexity in fault zones: examples from the San Andreas and Calaveras Faults. Geophys. J.R. astr. Soc. 79, 135-152.

Coulson S., Garth, T., Rietbrock, A., 2018. Velocity structure of the subducted Yakutat terrane, Alaska: insights from guided waves. Geophys. Res. Lett. 45, 3420-3428.

Dziewonski, A., Bloch, S., Landisman, M., 1969. A technique for the analysis of transient seismic signals. Bull. seism. Soc. Am. 59, 427–444.

Ellsworth, W.L., Malin, P.E., 2011. Deep rock damage in the San Andreas Fault revealed by P- and S-type fault-zone-guided waves. Geological Society, London, Special Publications 359, 39-53. doi:10.1144/SP359.3.

Fuchs, K., Müller, G., 1971. Computation of synthetic seismograms with the reflectivity method and comparison with observations. Geophys. J.R. astr. Soc. 23, 417-433.

Fielding, E.J., 1996. Tibet uplift and erosion. Tectonophysics 260, 55–84.

Fukao, Y., Hori, S., Ukawa, M., 1983. A seismological constraint on the depth of basalt-eclogite transition in a subducting oceanic crust. Nature 303, 413-415.

Garth, T., Rietbrock, A., 2014a. Order of magnitude increase in subducted H_2O due to hydrated normal faults within the Wadati-Benioff zone. Geology 42, 207-210. doi:10.1130/G34730.1.

Garth, T., Rietbrock, A., 2014b. Downdip velocity changes in subducted oceanic crust beneath Northern Japan – insights from guided waves. Geophys. J. Int. 198, 1342-1358. doi:10.1093/gji/ggu206.

Garth, T., Rietbrock, A., 2017. Constraining the hydration of the subducting Nazca plate beneath Northern Chile using subduction zone guided waves. Earth Planet. Sci. Lett. 474, 237-247. doi:10.1016/j.epsl.2017.06.041.

Haberland, C., Agnon, A., El-Kelani, R., Maercklin, N., Qabbani, I., Rümpker, G., Ryberg, T., Scherbaum, G., Weber, M., 2003. Modelling of seismic guided waves at the Dead Sea Transform. J. Geophys. Res. 108, 2342. doi:10.1029/2002JB002309.

Hacker, B., Luffi, P., Lutkov, V., Minaev, V., Ratschbacher, L., Plank, T., Ducea, M., Patino-Douce, A., McWilliams, M., Metcalf, J., 2005. Near-ultrahigh pressure proceesing of continental crust: Miocene crustal xenoliths from the Pamir. J. Petrol. 46, 1661-1687. doi:10.1093/petrology/egi030.

Hamburger, M.W., Sarewitz, D.R., Pavlis, T.L., Popandopulo, G.A., 1992. Structural and seismic evidence for intracontinental subduction in the Peter the First Range, Central Asia. Geol. Soc. Am. Bull. 104, 397-408.

Hori, S., 1990. Seismic waves guided by untransformed oceanic crust subducting into the mantle: the case of the Kanto district, central Japan. Tectonophysics 176, 355-376.

Jiménez-Munt, I., Fernàndez, M., Vergés, J., Platt, J.P., 2008. Lithosphere structure underneath the Tibetan Plateau inferred from elevation, gravity and geoid anomalies. Earth Planet. Sci. Lett. 267, 276-289.

Johnson, M.R.W., 2002. Shortening budgets and the role of continental subduction during the India–Asia collision. Earth-Science Reviews 59, 101-123.

Kelly, K.R., Ward, R.W., Treitel, S., Alford, R.M., 1976. Synthetic seismograms: a finite difference approach. Geophysics 41, 2-27.

Kind, R., Yuan, X., Saul, J., Nelson, D., Sobolev, S.V., Mechie, J., Zhao, W., Kosarev, G., Ni, J., Achauer, U., Jiang, M., 2002. Seismic images of crust and upper mantle beneath Tibet: Evidence for Eurasian plate subduction. Science 298, 1219-1221.

Kufner, S.-K., Schurr, B., Sippl, C., Yuan, X., Ratschbacher, L., Akbar, A. s/of M., Ischuk, A., Murodkulov, S., Schneider, F., Mechie, J., Tilmann, F., 2016. Deep India meets deep Asia: Lithospheric indentation, delamination and break-off under Pamir and Hindu Kush (Central Asia). Earth Planet. Sci. Lett. 435, 171-184. doi:10.1016/j.epsl.2015.11.046.

Kumar, P., Yuan, X., Kind, R., Ni, J., 2006. Imaging the colliding Indian and Asian lithospheric plates beneath Tibet. J. Geophys. Res. 111, B06308. doi:10.1029/2005JB003930.

Le Pichon, X., Fournier, M., Jolivet, L., 1992. Kinematics, topography, shortening, and extrusion in the India–Asia collision. Tectonics 11, 1085–1098.

Li, C., van der Hilst, R.D., Meltzer, A.S., Engdahl, E.R. 2008. Subduction of the Indian lithosphere beneath the Tibetan plateau and Burma. Earth Planet. Sci. Lett. 274, 157-168. doi:10.1016/j.epsl.2008.07.016.

Li, W., Chen, Y., Yuan, X., Schurr, B., Mechie, J., Oimahmadov, I., Fu, B., 2018. Continental lithospheric subduction and intermediate-depth seismicity: Constraints from S-wave velocity structures in the Pamir and Hindu Kush. Earth Planet. Sci. Lett. 482, 478-489. doi:10.1016/j.epsl.2017.11.031.

Li, Y.-G., Malin, P.E., 2008. San Andreas Fault damage at SAFOD viewed with fault-guided waves. Geophys. Res. Lett. 35, L08304. doi:10.1029/2007GL032924.

Martin, S., Rietbrock, A., Haberland, C., Asch, G., 2003. Guided waves propagating in subducted oceanic crust. J. Geophys. Res. 108, 2536. doi:10.1029/2005GL024183.

Martin, S., Haberland, C., Rietbrock., A., 2005. Forearc decoupling of guided waves in the Chile-Peru subduction zone. Geophys. Res. Lett. 32, L23309. doi:10.1029/2003JB002450.

Martin, S., Rietbrock, A., 2006. Guided waves at subduction zones: dependencies on slab geometry, receiver locations and earthquake sources. Geophys. J. Int. 167, 693-704. doi:10.1111/j.1365-246X.2006.02963.x.

Mechie, J., Kind, R., Saul, J., 2011. The seismological structure of the Tibetan plateau crust and mantle down to 700 km depth. In: Gloaguen, R. & Ratschbacher, L. (Eds.), Growth and Collapse of the Tibetan Plateau. Geological Society, London, Special Publications 353, 109-125.

Mechie, J., Yuan, X., Schurr, B., Schneider, F., Sippl, C., Ratschbacher, L., Minaev, V., Gadoev, M., Oimahmadov, I., Abdybachaev, U., Moldobekov, B., Orunbaev, S., Negmatullaev, S., 2012. Crustal and uppermost mantle velocity structure along a profile across the Pamir and southern Tien Shan as derived from project TIPAGE wide-angle seismic data. Geophys. J. Int. 188, 385-407. doi:10.1111/j.1365-246X.2011.05278.x.

Mechie, J., Kind, R., 2013. A model of the crust and mantle structure down to 700 km depth beneath the Lhasa to Golmud transect across the Tibetan plateau as derived from seismological data. Tectonophysics 606, 187-197. doi:10.1016/j.tecto.2013.04.030.

Negredo, A., Replumaz, A., Villaseñor A., Guillot, S., 2007. Modeling the evolution of continental subduction processes in the Pamir-Hindu Kush region. Earth Planet. Sci. Lett. 259, 212-225. doi:10.1016/j.epsl.2007.04.043.

Pavlis, G.L., Das, S., 2000. The Pamir-Hindu Kush seismic zone as a strain marker for flow in the upper mantle. Tectonics 19, 103-115.

Pegler, G., Das, S., 1998. An enhanced image of the Pamir–Hindu Kush seismic zone from relocated earthquake hypocenters. Geophys. J. Int. 134, 573–595.

Perry, M., Kakar, N., Ischuk, A. Metzger, S., Bendick, R., Molnar, P., Mohadjer, S., 2019. Little geodetic evidence for localized Indian subduction in the Pamir-Hindu Kush of central Asia. Geophys. Res. Lett. 46, 109–118. doi:10.1029/2018GL080065.

Podvin, P., Lecomte, I., 1991. Finite difference computation of traveltimes in very contrasted velocity models: a massively parallel approach and its associated tools. Geophys. J. Int. 105, 271-284.

Reynolds, A.C., 1978. Boundary conditions for the numerical solution of wave propagation problems. Geophysics 43, 1099-1110.

Rutte, D., Ratschbacher, L., Khan, J., Stübner, K., Hacker, B.R., Stearns, M.A., Enkelmann, E., Jonckheere, R., Pfänder, J.A., Sperner, B., Tichomirowa, M., 2017. Building the Pamir-Tibetan Plateau—Crustal stacking, extensional collapse, and lateral extrusion in the Central Pamir: 2. Timing and rates. Tectonics 36, 385–419. doi:10.1002/2016TC004294.

Sandmeier, K.-J., 1990. Untersuchung der Ausbreitungseigenschaften seismischer Wellen in geschichteten und streuenden Medien. PhD thesis, Karlsruhe University.

Schneider, W.A., Ranzinger, K.A., Balch, A.H., Kruse, C., 1992. A dynamic programming approach to first arrival traveltime computation in media with arbitrarily distributed velocities. Geophysics 57, 39-50.

Schneider, F. M., Yuan, X., Schurr, B., Mechie, J., Sippl, C., Haberland, C., Minaev, V., Oimahmadov, I., Gadoev, M., Radjabov, N., Abdybachaev, U., Orunbaev, S., Negmatullaev, S., 2013. Seismic imaging of subducting continental lower crust beneath the Pamir. Earth Planet. Sci. Lett. 375, 101-112. doi:10.1016/j.epsl.2013.05.015.

Schurr, B., Ratschbacher, L., Sippl, C., Gloaguen, R., Yuan, X., Mechie, J., 2014a. Seismotectonics of the Pamir. Tectonics 33, 1501-1518. doi:10.1002/2014TC003576.

Schurr, B., Haberland, C., Sippl, C., Yuan, X., Mechie, J., Schneider, F., Team, T., 2014b. Imaging continental collision and subduction in the Pamir mountain range, Central Asia, by seismic attenuation tomography. Geophysical Research Abstracts 16, EGU2014-13637, EGU General Assembly 2014.

Schwab, M., Ratschbacher, L., Siebel, W., McWilliams, M., Minaev, V., Lutkov, V., Chen, F., Stanek, K., Nelson, B., Frisch, W., Wooden, J.L., 2004. Assembly of the Pamirs: Age and origin of magmatic belts from the southern Tien Shan to the southern Pamirs and their relation to Tibet. Tectonics 23, TC4002. doi:10.1029/2003TC001583.

Shaffer, M., Hacker, B.R., Ratschbacher, L., Kylander-Clark, A.R.C. 2017. Foundering triggered by the collision of India and Asia captured in xenoliths. Tectonics 36, 1913–1933. doi:10.1002/2017TC004704.

Sippl, C., Schurr, B., Yuan, X., Mechie, J., Schneider, F.M., Gadoev, M., Orunbaev, S., Oimahmadov, I., Haberland, C., Abdybachaev, U., Minaev, V., Negmatullaev S., Radjabov, N., 2013a. Geometry of the Pamir-Hindu Kush intermediate-depth earthquake zone from local seismic data. J. Geophys. Res. 118, 1438-1457. doi:10.1002/jgrb.50128.

Sippl, C., Schurr, B., Tympel, J., Angiboust, S., Mechie, J., Yuan, X., Schneider, F.M., Sobolev, S.V., Ratschbacher, L., Haberland, C., TIPAGE-Team, 2013b. Deep burial of Asian continental crust beneath the Pamir imaged with local earthquake tomography. Earth Planet. Sci. Lett. 384, 165-177. doi:10.1016/j.epsl.2013.10.013.

Stolper, E., Walker, D., Hager, B.H., Hays, J.F., 1981. Melt segregation from partially molten source regions: the importance of melt density and source region size. J. Geophys. Res. 86, 6261-6271.

Vidale, J., 1988. Finite-difference calculation of travel times. Bull. Seismol. Soc. America. 78, 2062-2076.

Watt, J.P., Davies, G.F., O'Connell, R.J., 1976. The elastic properties of composite materials. Rev. Geophys. Space Phys. 14, 541-563.

Wessel, P., Smith, W.H.F., 1991. Free software helps map and display data. EOS Trans. AGU 72, 441.

Wu, J., Hole, J.A., Snoke, J.A., 2010. Fault zone structure at depth from differential dispersion of seismic guided waves: evidence for a deep waveguide on the San Andreas Fault. Geophys. J. Int. 182, 343-354. doi: 10.1111/j.1365-246X.2010.04612.x.

Yin, A., Harrison, T.M., 2000. Geologic evolution of the Himalayan-Tibetan orogen. Annu. Rev. Earth Planet. Sci. 28, 211-280.

Yuan, X., Mechie, J., Schurr, B., 2008. Tienshan Pamir Geodynamics Project (TIPAGE). Deutsches GeoForschungsZentrum GFZ. Other/Seismic Network. doi:10.14470/2O097102.

Zhao, J., Yuan, X., Liu, H., Kumar, P., Pei, S., Kind, R., Zhang, Z., Teng, J., Ding, L., Gao, X., Xu, Q., Wang, W., 2010. The boundary between the Indian and Asian tectonic plates below Tibet. Proceedings National Academy of Sciences 107, 11229-11233. doi:10.1073/pnas.1001921107.

Table 1
Click here to download Table: casia055_tab1_rev.xls

Table 1. Origin time, hypocentre and local magnitude M_L for each of the 13 events used in this study. The origin times and hypocentres have been derived by relocating the events in the 3-D model of Sippl et al. (2013b).

event	origin time year:day of year:hour:min:sec	longitude °E	latitude °N	depth km	M_L
302	2008:281:03:46:51.850	74.0620	38.1937	158.5	4.5
304	2008:304:10:52:17.430	73.9187	38.3563	125.8	3.8
314	2008:242:19:48:18.930	73.9827	38.1557	163.9	3.3
315	2009:081:00:17:19.730	74.1722	38.1535	165.0	3.0
317	2009:004:07:50:40.850	74.0317	38.1773	156.2	3.0
318	2008:246:16:52:45.190	74.0813	38.1922	156.1	3.9
319	2008:225:22:53:57.630	74.1098	38.1973	152.7	3.5
321	2009:098:16:42:28.800	74.1167	38.2305	148.5	3.7
325	2009:139:01:48:19.070	73.9970	38.3682	128.1	3.8
326	2008:231:14:13:44.180	73.9935	38.3705	126.9	3.8
327	2009:003:17:09:20.860	73.9092	38.3747	124.5	3.5
328	2009:057:07:50:49.150	73.9773	38.3677	129.6	5.2
330	2009:086:21:15:35.400	73.8485	38.4397	105.0	4.1

Figure 1

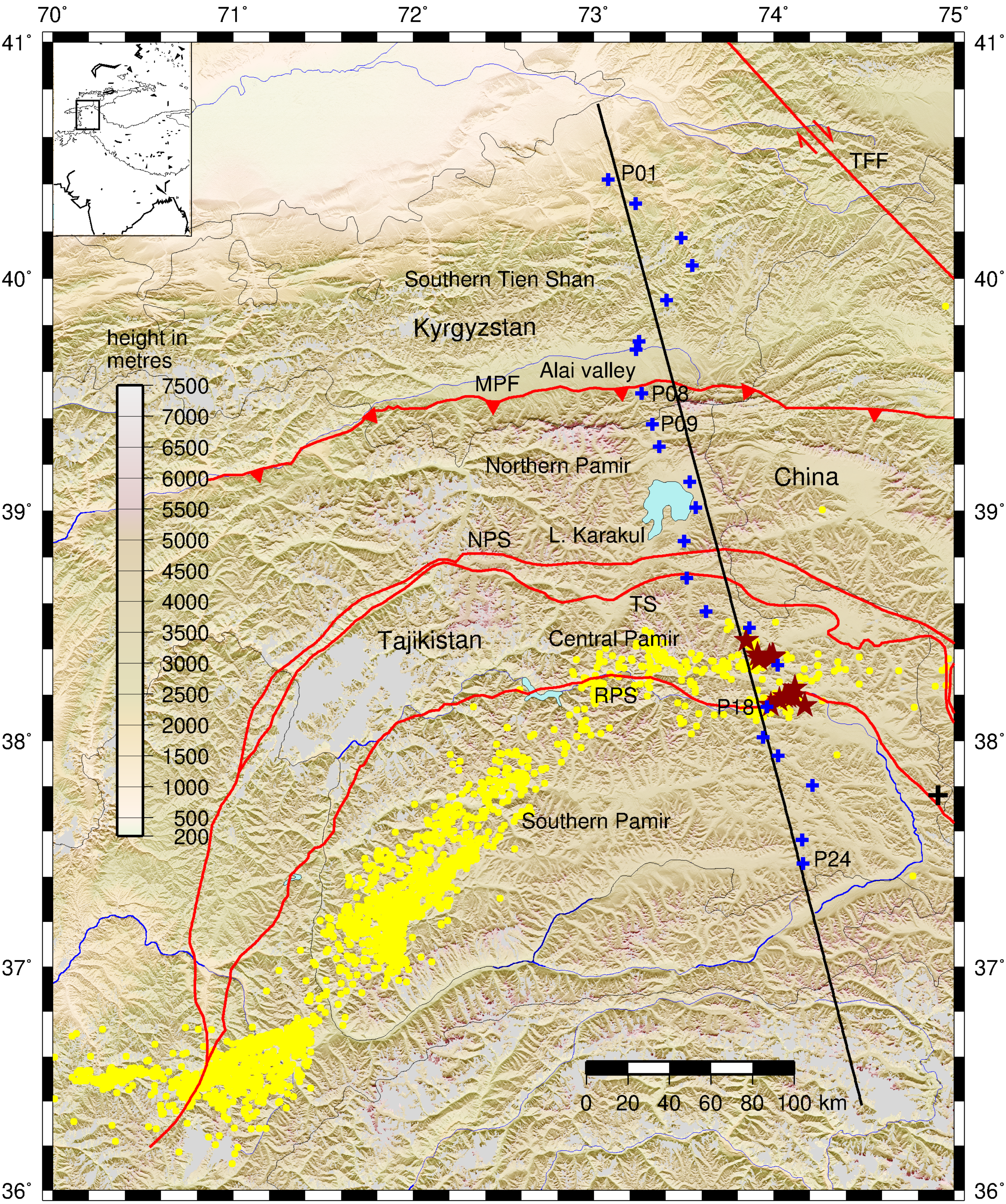

Fig. 1. Location map of the seismological stations (blue crosses) along the TIPAGE main profile (black line) and the 13 earthquakes (dark red stars) used in this study. The Pamir – Hindu Kush seismic zone delineated by earthquakes at depths greater than 90 km from the catalogue of Sippl et al. (2013a) is shown by yellow dots. The xenolith locality of Hacker et al. (2005) in the southeastern Pamir is marked by a black cross. The topography is from the Shuttle Radar Topography Mission (SRTM). In the inset the outline of Tibet, the Pamir and the Tien Shan, as defined by the 3000 m contour, is shown. Key: MPF – Main Pamir Fault, NPS – Northern Pamir Suture, TS – Tanymas Suture, RPS – Rushan Pshart Suture, TFF – Talas Fergana Fault.

Figure 2

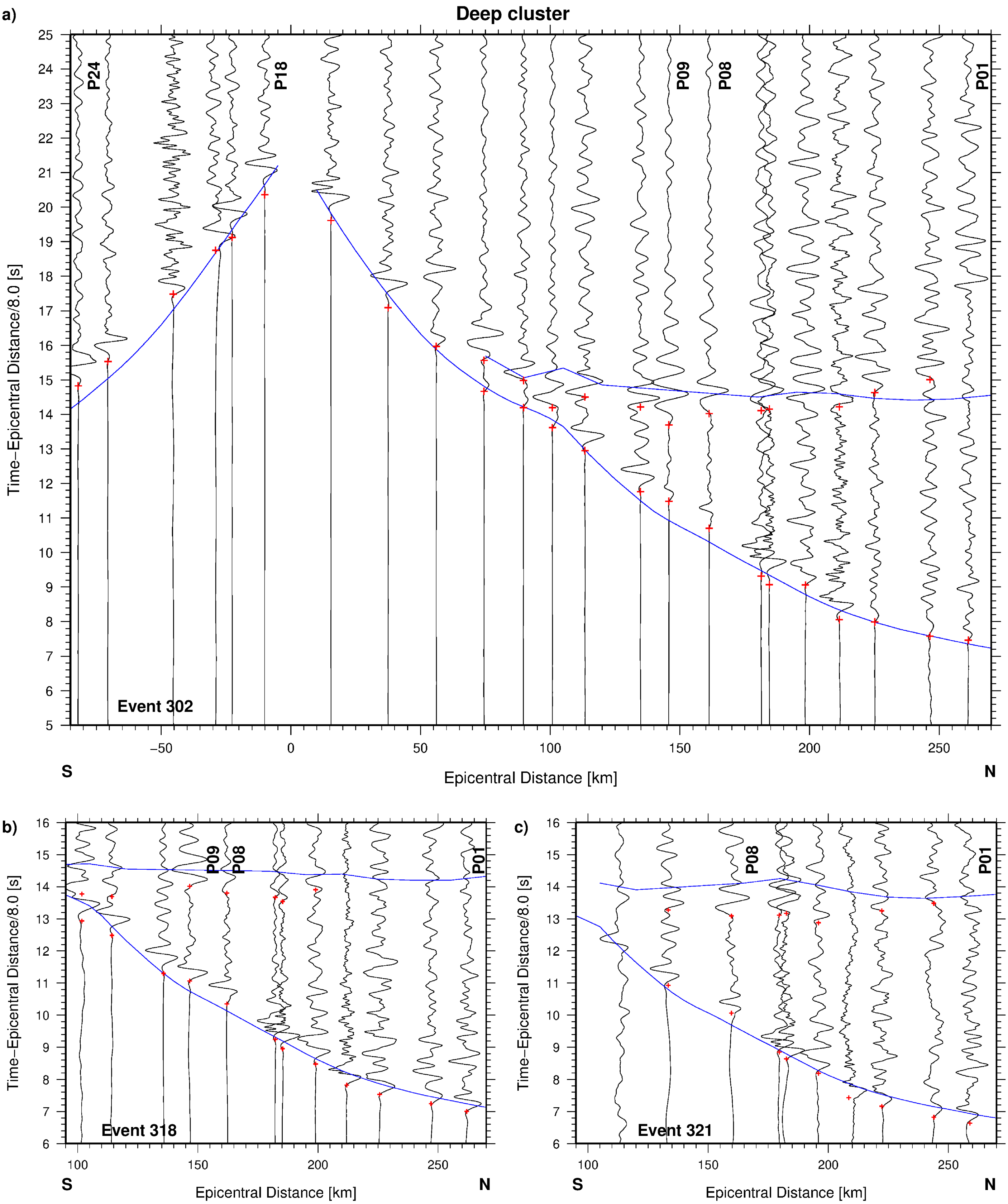

Fig. 2. Observations of guided waves from the deep cluster of earthquakes. Data from events a) 302, b) 318 and c) 321 are shown. The record sections show the vertical component of motion reduced with a velocity of 8 km/s. Each trace is normalized individually and is bandpass filtered from 0.1 to 2 Hz. The red crosses mark the picked 1st arrivals and 2nd arrivals of the guided waves. The blue lines mark the theoretical 1st arrivals and 2nd arrivals of the guided waves from model 2 shown in Fig. 6. The traces recorded by stations which are labelled in Fig. 1, including P08 and P09 for which the dispersion analysis was carried out, are also marked.

Figure 3

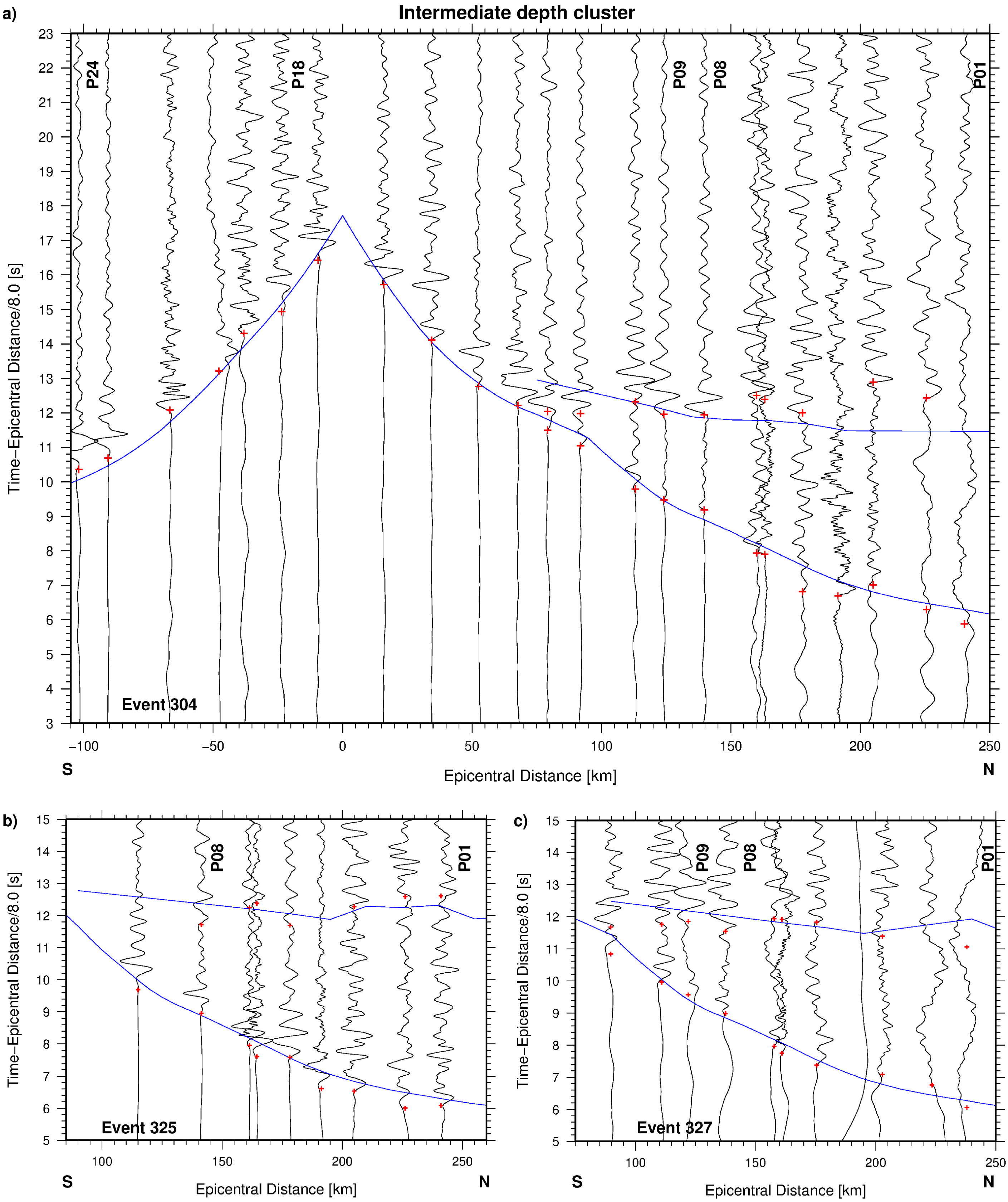

Fig. 3. Observations of guided waves from the intermediate cluster of earthquakes. Data from events a) 304, b) 325 and c) 327 are shown. The data are processed and presented as in Fig. 2.

Figure 4

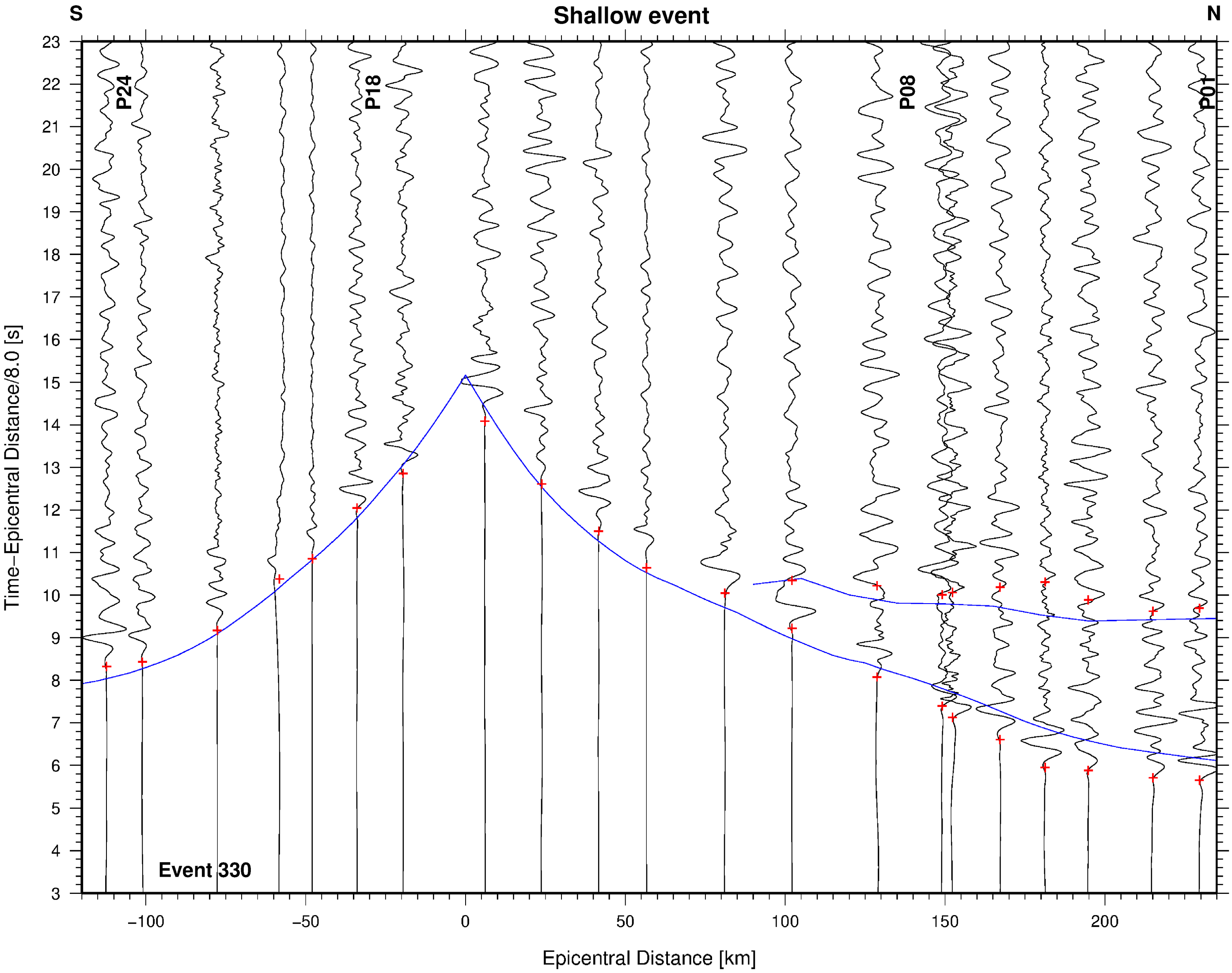

Fig. 4. Observations of guided waves from the shallow event, 330. The data are processed and presented as in Fig. 2.

Figure 5

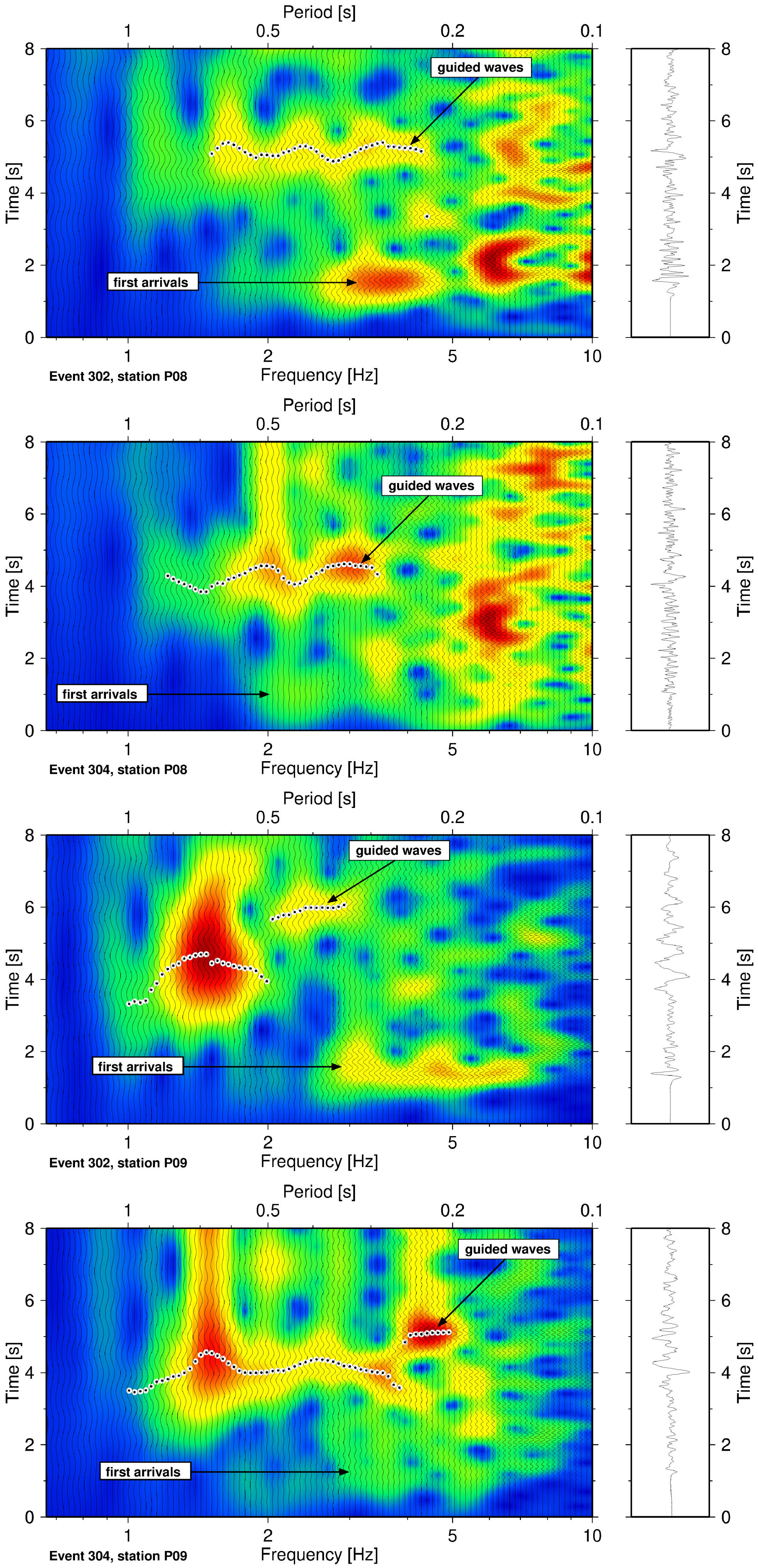

Fig. 5. Frequency (period) versus time plots for the P−wavefield recorded by the vertical component at two stations (P08 & P09, Figs. 2−3) for two events (302 & 304, Table 1). In each case, the analysed seismogram is shown to the right of the frequency−time plot and the dots mark the frequency−dependent arrival time of the guided waves. The locations of the events and stations are marked in Figs. 1, 6 and 7 and the relevant traces are also marked in Figs. 2a and 3a.

Figure 6

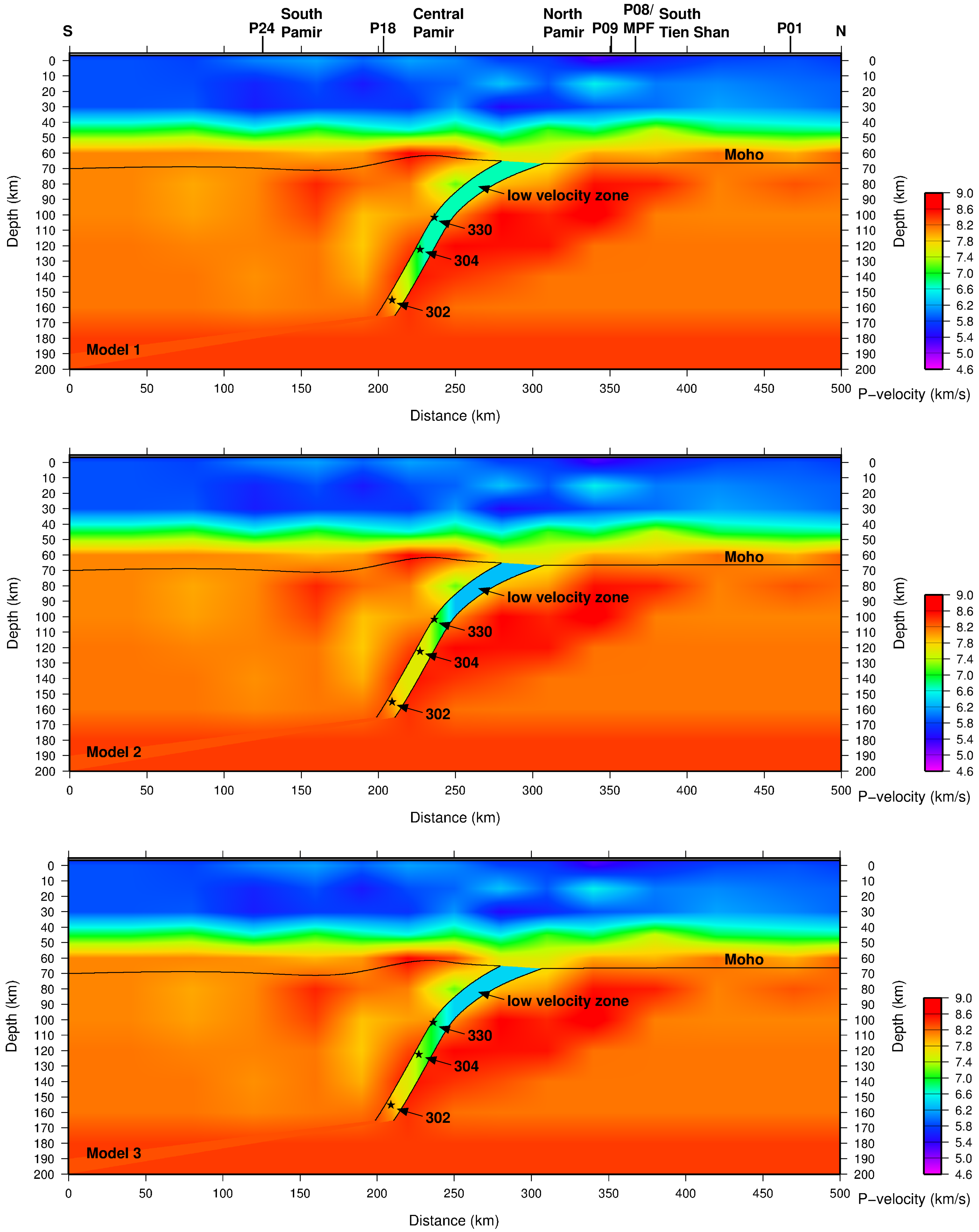

Fig. 6. Velocity models along the TIPAGE main profile (black line in Fig. 1) with a low velocity zone (LVZ) in the mantle producing guided waves. In model 1 (upper plot) the LVZ has a velocity of 6.7 km/s at depths shallower than about 130 km. In model 2 (middle plot) the velocities in the LVZ are such that the velocity above the shallow earthquake has a value of 6.3 km/s, and the velocity between the shallow earthquake and the deep earthquakes has a value of 7.6 km/s. In model 3 (lower plot) the velocity in the LVZ above the shallow earthquake was assigned a value of 6.4 km/s, the velocity between the shallow earthquake and the intermediate cluster of earthquakes was assigned a value of 7.2 km/s and the velocity between the intermediate and deep clusters of earthquakes was assigned a value of 7.6 km/s. The theoretical 1st arrivals and 2nd arrivals of the guided waves for model 2 are shown for various events in Figs. 2–4. The Moho between 60 and 70 km depth is after Schneider et al. (2013) and there is no vertical exaggeration. Stations labelled in Fig. 1 are also marked. Key: see Fig. 1.

Figure 7

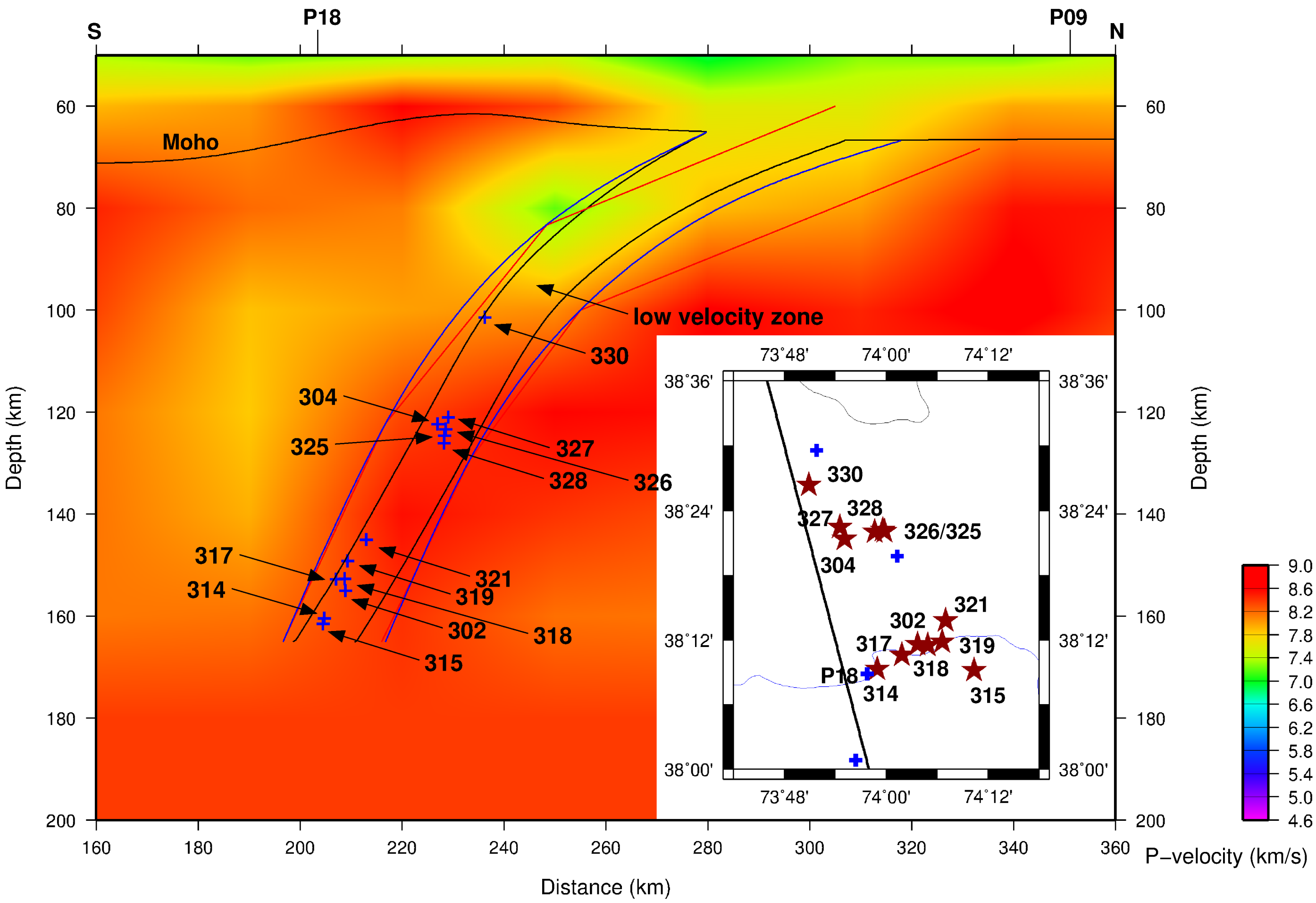

Fig. 7. The 13 events (see also large–scale inset map) from the Pamir seismic zone which showed guided waves and were used in this study in relation to the boundaries of the low velocity zone (LVZ) and the background velocity model (see also cross–section D–D' in Fig. 2 of Sippl et al., 2013b). The red lines are the boundaries of the LVZ shown in Schneider et al. (2013) while the blue and black lines are the boundaries of the LVZ used in this study (blue – initial, test models, black – later models) and also shown in Figs. 6 and S1–S2. The Moho between 60 and 70 km depth is after Schneider et al. (2013) and there is no vertical exaggeration. Stations labelled in Fig. 1 are also marked.

Figure 8

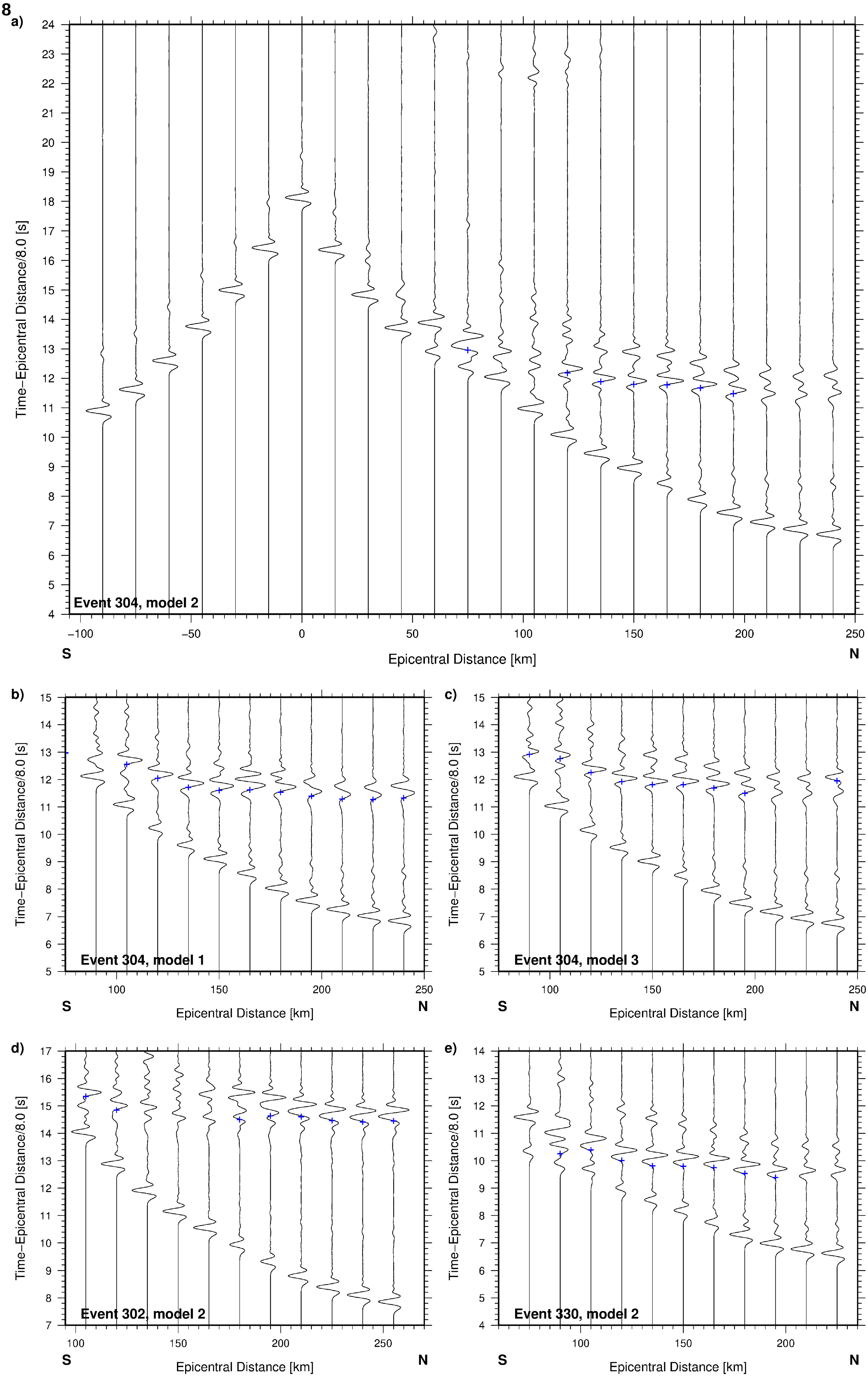

Fig. 8. Synthetic seismograms for event 304 for a) model 2, b) model 1 and c) model 3 and for events d) 302 and e) 330 for model 2. Models 1, 2 and 3 are described and shown in Fig. 6. The blue crosses mark the picked arrivals of the guided waves. The synthetic seismograms which show the vertical component of motion, were calculated for an explosive point source with a dominant frequency of 1.5 Hz. The record sections are reduced with a velocity of 8 km/s and each trace is normalized individually.

Figure 9

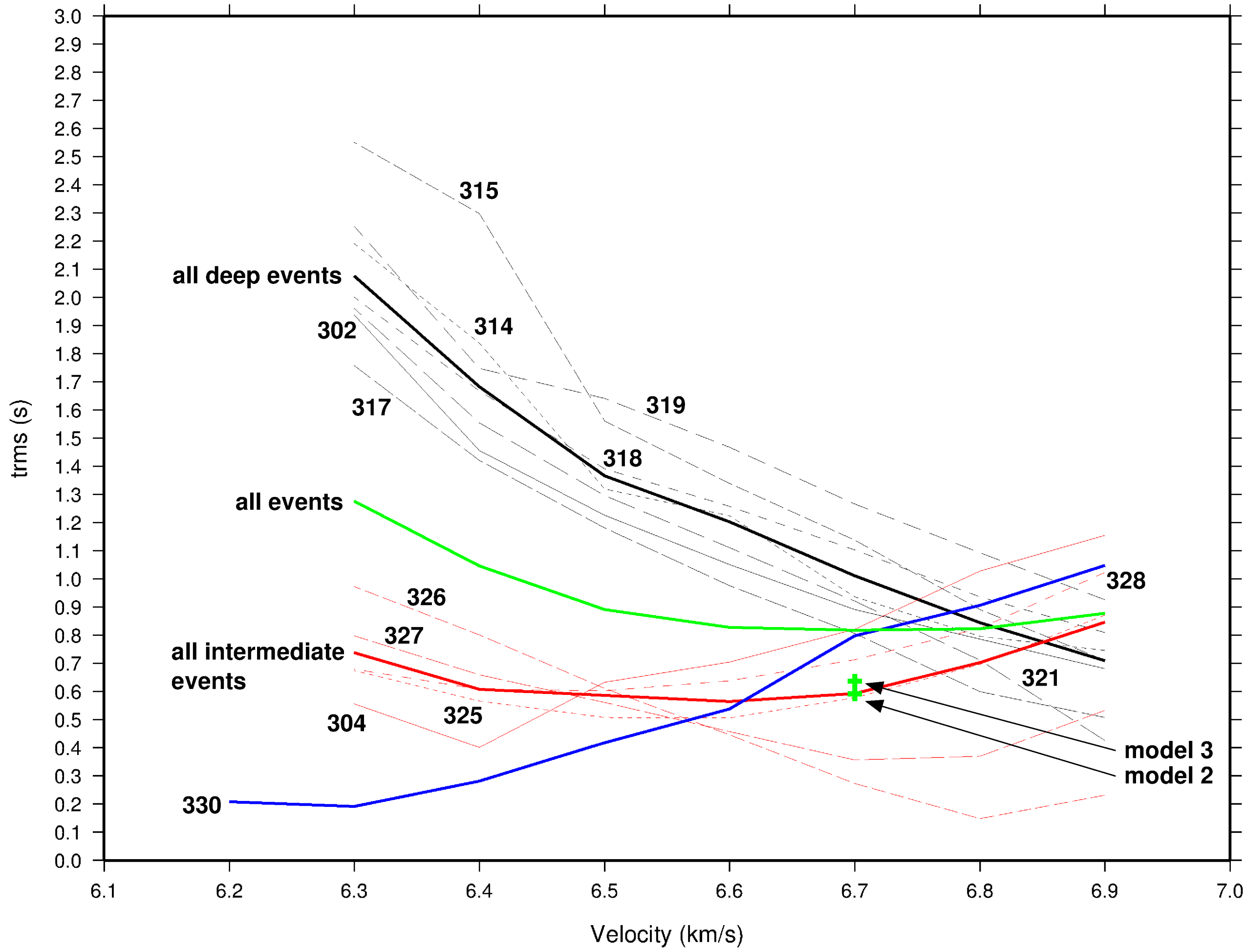

Fig. 9. Plot of root mean square travel−time residuals (trms) against the velocity in the low velocity zone at depths shallower than 130 km. For each of the 13 events, the event no. is plotted beside the line. Additionally, lines are shown for the five intermediate events (thick red line), the seven deep events (thick black line) and for all events (thick green line), and green crosses, plotted at the somewhat arbitrary velocity value of 6.7 km/s, are shown for models 2 and 3. For a description of models 2 and 3, see Fig. 6.

Figure 10

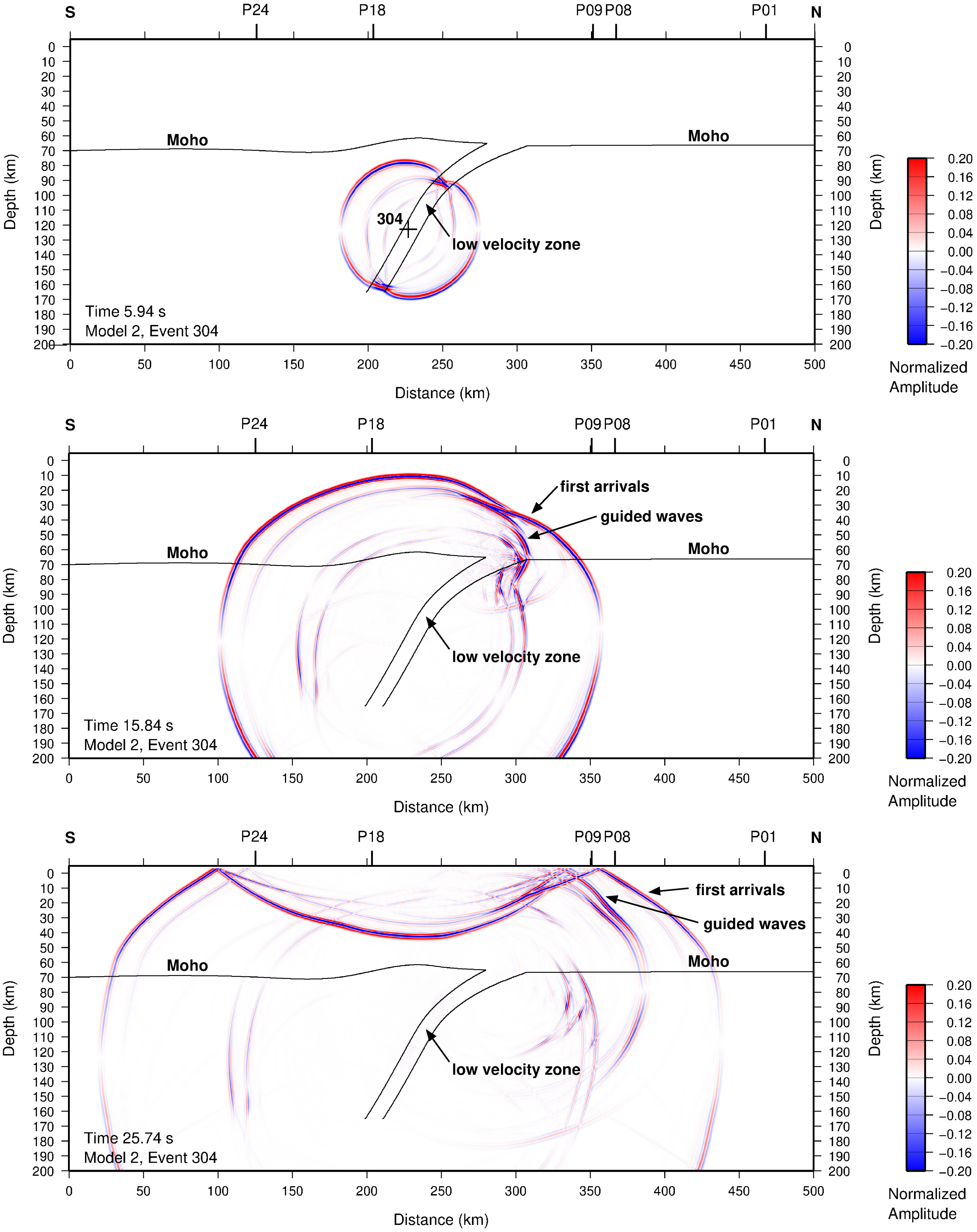

Fig. 10. Snapshots of waves propagating from event 304 through model 2 (Fig. 6). The snapshots are shown for 5.94 s (top), 15.84 s (middle) and 25.74 s (bottom) after the origin time of the event. The boundaries of the low velocity zone are marked as is the Moho between 60 and 70 km depth after Schneider et al. (2013). There is no vertical exaggeration. Stations labelled in Fig. 1 are also marked. An animation of this example is shown as Video S1.

Figure 11

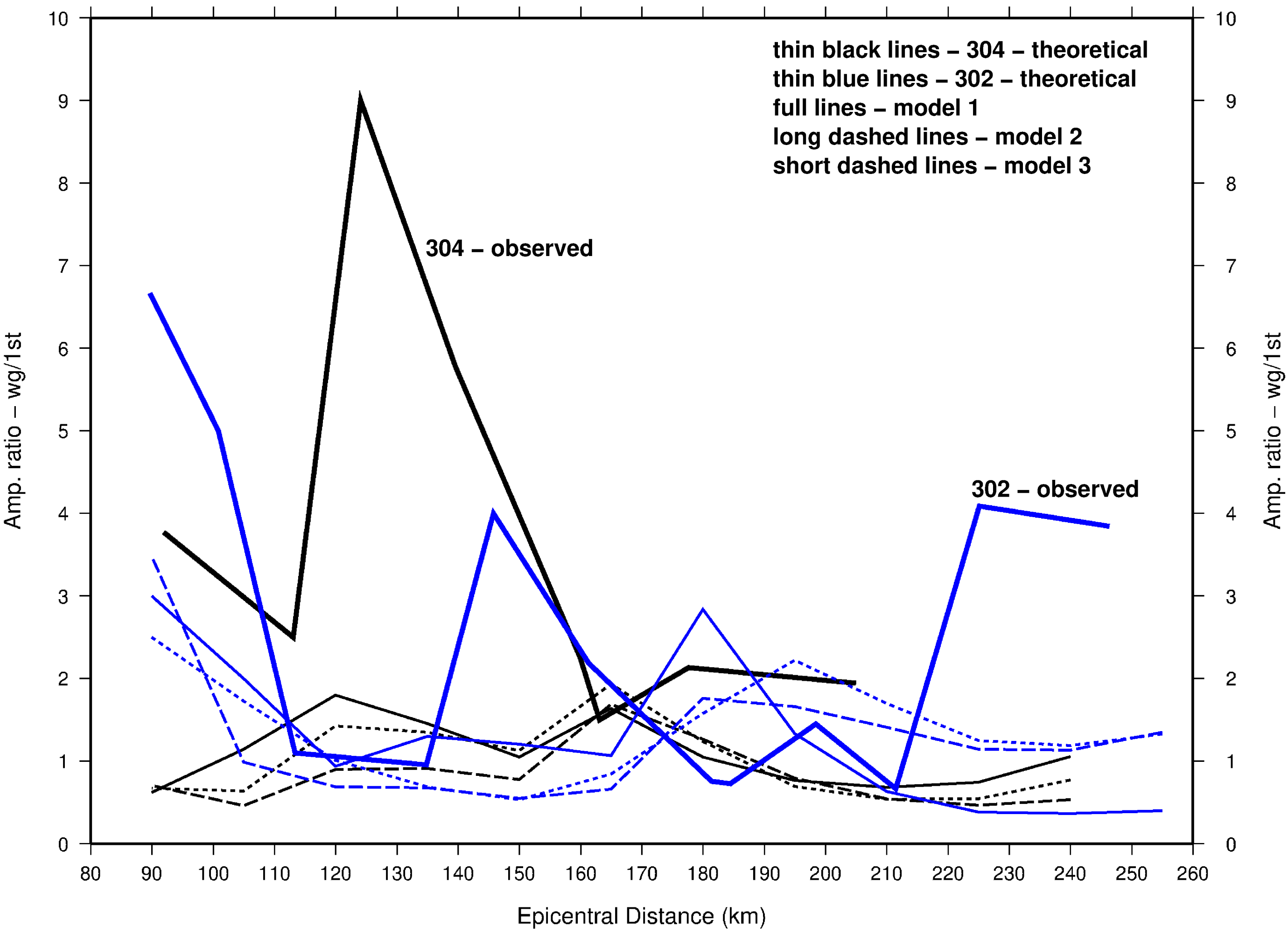

Fig. 11. Plot of amplitude ratios between the guided waves and the 1st arrivals (Amp. ratio – wg/1st) against the epicentral distance for the two events 302 and 304 and for the models 1–3 defined in Fig. 6. The theoretical amplitude ratios from models 1–3 are marked by thin blue lines for event 302 and thin black lines for event 304, while the observed amplitude ratios for events 302 and 304 are marked by thick blue and black lines respectively. Large amplitude ratios mean high amplitude guided waves with respect to the amplitudes of the 1st arrivals.

Figure 12

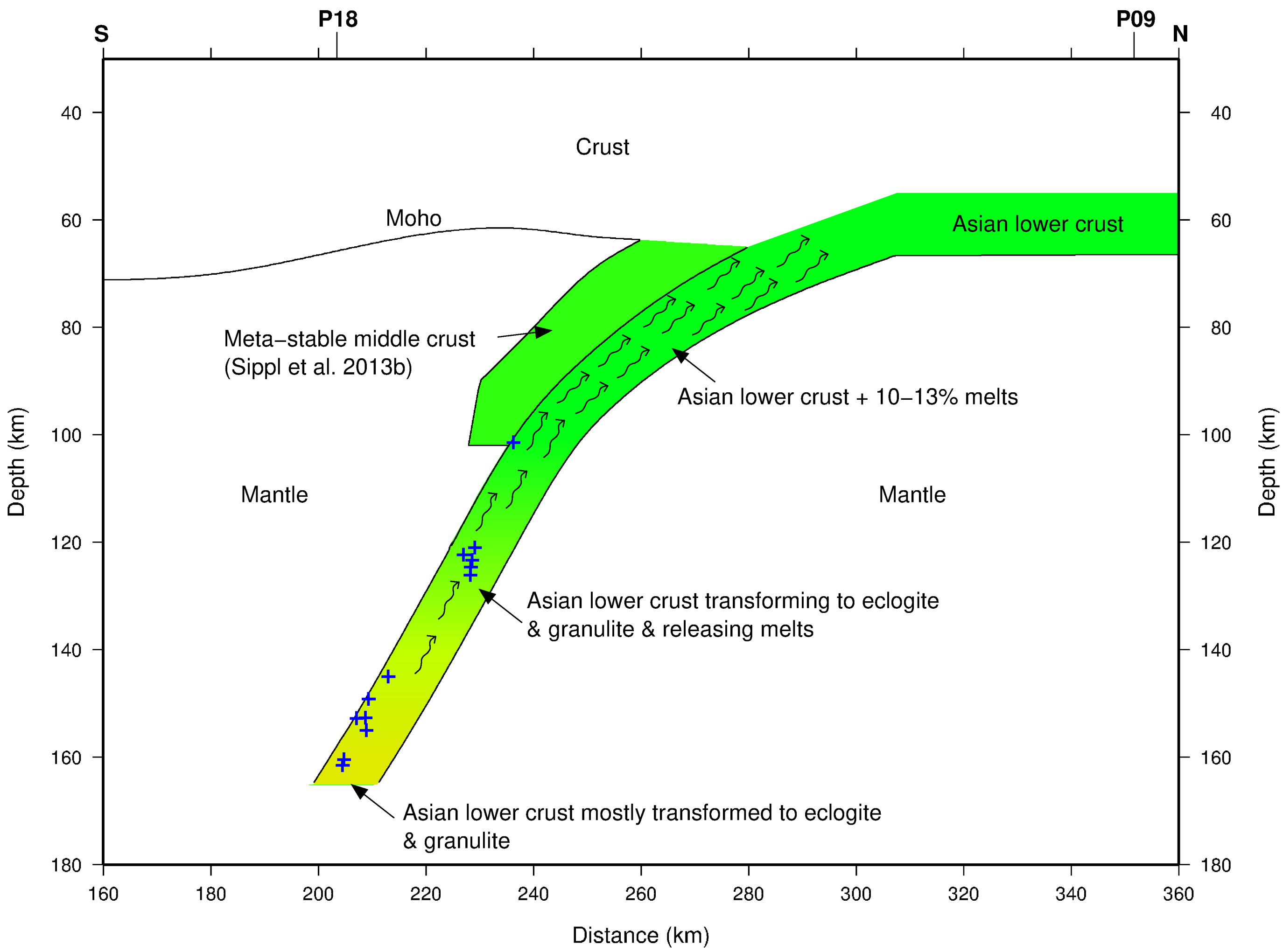

Fig. 12. Schematic diagram of the subduction of Asian crust within the Pamir seismic zone and the transformation of the lower crust to eclogite and granulite accompanied by the release of melts. The meta−stable middle crust is shown after Sippl et al. (2013b). Blue crosses mark the locations of the 13 events showing good guided waves used in this study. The melts are thought to be confined to the zone where the lower crust is subducting for density reasons.